Upper-Ocean Dynamical Features and Prediction of the Super El Niño in 2015/16: A Comparison with the Cases in 1982/83 and 1997/98

Hong-Li REN[1,3*], Run WANG[1,2], Panmao ZHAI[2], Yihui DING[1], and Bo LU[1,3]

1 *Laboratory for Climate Studies*, *National Climate Center*, *China Meteorological Administration*, *Beijing* 100081
2 *Chinese Academy of Meteorological Sciences*, *Beijing* 100081
3 *CMA–NJU Joint Laboratory for Climate Prediction Studies*, *School of Atmospheric Sciences*, *Nanjing University*, *Nanjing* 210023

(Received October 31, 2016; in final form January 16, 2017)

ABSTRACT

The 2015/16 super El Niño event has been widely recognized as comparable to the 1982/83 and 1997/98 El Niño events. This study examines the main features of upper-ocean dynamics in this new super event, contrasts them to those in the two historical super events, and quantitatively compares the major oceanic dynamical feedbacks based on a mixed-layer heat budget analysis of the tropical Pacific. During the early stage, this new event is characterized by an eastward propagation of SST anomalies and a weak warm-pool El Niño; whereas during its mature phase, it is characterized by a weak westward propagation and a westward-shifted SST anomaly center, mainly due to the strong easterly wind and cold upwelling anomalies in the far eastern Pacific, as well as the westward anomalies of equatorial zonal current and subsurface ocean temperature. The heat budget analysis shows that the thermocline feedback is the most crucial process inducing the SST anomaly growth and phase transition of all the super events, and particularly for this new event, the zonal advective feedback also exerts an important impact on the formation of the strong warming and westward-shifted pattern of SST anomalies. During this event, several westerly wind burst events occur, and oceanic Kelvin waves propagate eastwards before being maintained over eastern Pacific in the mature stage. Meanwhile, there is no evidence for westward propagation of the off-equatorial oceanic Rossby waves though the discharging process of equatorial heat during the development and mature stages. The second generation El Niño prediction system of the Beijing Climate Center produced reasonable event real-time operational prediction during 2014–16, wherein the statistical prediction model that considers the preceding oceanic precursors plays an important role in the multi-method ensemble prediction of this super.

Key words: El Niño–Southern Oscillation, super El Niño event, ocean dynamics, feedback, prediction

Citation: Ren, H.-L., R. Wang, P. M. Zhai, et al., 2017: Upper-ocean dynamical features and prediction of the super El Niño in 2015/16: A comparison with the cases in 1982/83 and 1997/98. *J. Meteor. Res.*, **31**(2), 278–294, doi: 10.1007/s13351-017-6194-3.

1. Introduction

Many studies have shown that the El Niño–Southern Oscillation (ENSO) has a significant effect on global weather and climate, and as one of the dominant preceding signals for East Asian climate anomalies, has significant importance for short-term climate prediction in China (Li, 1990; Zhang et al., 1996; Wang et al., 2000; Chen, 2002; Zhang et al., 2011, 2012). For instance, the 1997/98 super El Niño event had a crucial impact on the occurrence of the severe flooding over the Yangtze River valley in the summer of 1998 (National Climate Center 1998; Huang et al., 2000). It has also been suggested that ENSO can indirectly affect climate in East Asia through interacting with the tropical Pacific annual cycle and tropical Indian Ocean air–sea interaction (Stuecker et al., 2013; Xie et al., 2016). Therefore, the dynamics and predictability of ENSO have long been and remain hot topics in scientific research.

A number of studies have focused on ENSO dynamics (Neelin et al., 1998; Chang et al., 2006, and references therein) and shown that the air–sea interaction, es-

Supported by the China Meteorological Administration Special Public Welfare Research Fund (GYHY201506013), National Natural Science Foundation of China (41606019, 41605116, and 41405080), and Project for Development of Key Techniques in Meteorological Operation Forecasting (YBGJXM201705).

*Corresponding author: renhl@cma.gov.cn.

pecially the oceanic dynamical feedback mechanisms, is crucial to the amplitude and phase transition of ENSO (e.g., Suarez and Schopf, 1988; Battisti and Hirst, 1989; Cane et al., 1990; Jin, 1997; Picaut et al., 1997; Weisberg and Wang 1997; Chao et al., 2002; Li et al., 2008). The thermocline feedback and zonal advective feedback, which are the two major dynamical feedbacks in ENSO evolution, make positive contributions to ENSO's growth and can be integrated into the recharge oscillator mechanism (Jin and An, 1999). On the basis of ENSO dynamics, it has become possible to predict sea surface temperature (SST) anomalies at lead times of several months by capturing early signals in the upper ocean (Meinen and McPhaden, 2000). Further studies on the oceanic dynamics of ENSO will help to improve our understanding of its mechanisms and predictability.

Recent studies have reported that the 2015/16 El Niño event was another super event, besides those of 1982/83 and 1997/98 (these three events are denoted 15/16, 82/83, and 97/98 hereafter), and research on their diagnosis, prediction and attribution has advanced well (Min et al., 2015; Chen H. C. et al., 2016; Chen S. F. et al., 2016; Gasparin and Roemmich, 2016; Hu and Fedorov, 2016; Levine and McPhaden, 2016; Li and Min, 2016; Liu et al., 2016; Ren et al., 2016b; Shao and Zhou, 2016; Stramma et al., 2016; Yuan et al., 2016; Zhai et al., 2016). The signals of this event appeared in early 2014, and after a series of fluctuations, it eventually developed into a super event at the end of 2015. One of the most remarkable features of this event is the westward shift of its SST anomaly center during the mature stage, compared with the previous two super events. The SST anomalies and atmospheric variables of this event have been extensively analyzed in these recent studies.

The present study focuses on diagnosing the upper-ocean dynamical features of this new super event, with the aim to identify which ocean feedback processes were the main factors in the formation of this event. Furthermore, we review the operational predictions of the Beijing Climate Center (BCC) by using oceanic precursors. Our work involves quantitatively comparing the 15/16 El Niño event with the 82/83 and 97/98 events, in terms of their upper-ocean evolutions and dynamics. Following this introduction, the data and methods used in the study are introduced in Section 2. The main features and upper-ocean dynamical features of the three super events are compared in Sections 3 and 4. An oceanic mixed-layer heat budget analysis is conducted in Section 5, and the predictions of the super events using the BCC's operational system [System of ENSO Monitoring, Analysis, and Prediction, version 2.0 (SEMAP2.0)] are reviewed in Section 6. Finally, a summary and discussion are given in Section 7.

2. Data and methods

The data used in the study are as follows:

(1) Monthly mean SST data from the Hadley Centre Sea Ice and Sea Surface Temperature dataset (HadISST) on a 1° × 1° horizontal grid (Rayner et al., 2003).

(2) Monthly ocean temperature and ocean circulation data from the Global Ocean Data Assimilation System (GODAS) of NCEP on a 1/3° latitude × 1° longitude horizontal grid (Behringer and Xue, 2004).

(3) Ocean surface current data (averaged over 0–30 m) from the Ocean Surface Current Analyses-Real Time (OSCAR) dataset at 5-day intervals and on a 1/3° × 1/3° horizontal grid (Bonjean and Lagerloef, 2002), which covers the period from November 1992 to August 2016.

(4) Monthly wind data at 1000 hPa from the NCEP–DOE (Department of Energy) Reanalysis 2 on a 2.5° × 2.5° horizontal grid (Kanamitsu et al., 2002).

(5) Niño indices, including Niño3 (5°S–5°N, 150°–90°W) and Niño3.4 (5°S–5°N, 170°–120°W), provided by the Climate Prediction Center/National Oceanic and Atmospheric Administration (CPC/NOAA) and computed by using data from the Extended Reconstructed Sea Surface Temperature dataset, version 4 (ERSSTv4), and the Optimum Interpolation Sea Surface Temperature dataset, version 2 (OISSTv2).

The climatology is taken as the period 1981–2010.

A heat budget analysis is used in this study for quantitatively diagnosing the relative importance of different dynamical feedbacks in the three super events. The methodology is consistent with previous studies (e.g., Zhang et al., 2007; Ren and Jin, 2013), based on the GODAS reanalysis data. Neglecting the second-order nonlinear terms, the mixed-layer averaged ocean temperature tendency equation can be generally expressed as

$$\frac{\partial T'}{\partial t} = -\left(\bar{u}\frac{\partial T'}{\partial x} + \bar{v}\frac{\partial T'}{\partial y} + \bar{w}\frac{\partial T'}{\partial z} + u'\frac{\partial \overline{T}}{\partial x} + v'\frac{\partial \overline{T}}{\partial y} + w'\frac{\partial \overline{T}}{\partial z}\right) + Q, \tag{1}$$

where T', u', v', and w' denote the ocean temperature and anomalies of currents, respectively, and Q stands for the thermal forcing. The over barred variables denote the climatological mean state. Particularly, the third term on the right-hand side of Eq. (1) can be further decomposed into an approximation,

$$-\bar{w}\frac{\partial T'}{\partial z} = \bar{w}\frac{T'_{\rm sub}}{H} - \bar{w}\frac{T'}{H}, \tag{2}$$

where H is the effective mean mixed-layer depth for the vertical advection, taken as a constant (50 m) in this study. The subscript "sub" denotes a subsurface-layer average between 50 and 100 m. By referring to Ren and Jin (2013), the right-hand side of Eq. (1) is divided into five linear feedback terms:

$$\frac{\partial T'}{\partial t} = {\rm MC} + {\rm ZA} + {\rm EK} + {\rm TH} + {\rm TD} + R, \tag{3}$$

where

$${\rm MC} = -\bar{u}\frac{\partial T'}{\partial x} - \bar{v}\frac{\partial T'}{\partial y} - \bar{w}\frac{T'}{H}, \tag{4}$$

$${\rm ZA} = -u'\frac{\partial \overline{T}}{\partial x}, \tag{5}$$

$${\rm EK} = -v'\frac{\partial \overline{T}}{\partial y} - w'\frac{\partial \overline{T}}{\partial z}, \tag{6}$$

$${\rm TH} = \bar{w}\frac{T'_{\rm sub}}{H}, \tag{7}$$

$${\rm TD} = Q. \tag{8}$$

Generally speaking, in these terms, MC denotes the effect of mean circulation damping, ZA denotes the zonal advective feedback, EK denotes the Ekman pumping feedback, TH denotes the thermocline feedback, TD denotes the thermodynamical damping, and R denotes the residual terms. Among them, the ZA, EK, and TH terms are the three major dynamic feedbacks, and make positive contributions to the growth of ENSO, while the MC and TD terms make negative contributions.

3. Main features of the three super El Niño events

Figure 1 compares the temporal evolutions of the equatorial SST anomalies of the three super events. The 82/83 and 97/98 event features are very similar to one another in that they both experienced rapid development stages, with positive SST anomaly centers located in the Niño3 region over eastern Pacific during their mature phase. The 15/16 event, which was more complicated and quite different from the previous two events, has a much longer life cycle (Zhai et al., 2016). The SST anomalies turned positive in early 2014 in the whole equatorial Pacific, and in the winter of 2014/15 were characterized by a weak central Pacific El Niño event. In 2015, this El Niño grew rapidly and was accompanied by a clear transformation from central-Pacific type to eastern-Pacific type. Particularly, the positive SST anomaly center of the 15/16 event was located in the Niño3.4 region during the mature stage, which was obviously more westward than in the previous two events. Therefore, when using the Niño3.4 index as the standard, the 15/16 event is strongest among the three super events (Table 1). In contrast, when using the Niño3 index as the standard, it is the weakest (Table 2). Furthermore, the peak times and values of the three super events based on different SST datasets also show some evident differences.

During the development stage of all three super events, the positive SST anomalies tended to propagate from the west to the east of the equatorial Pacific.

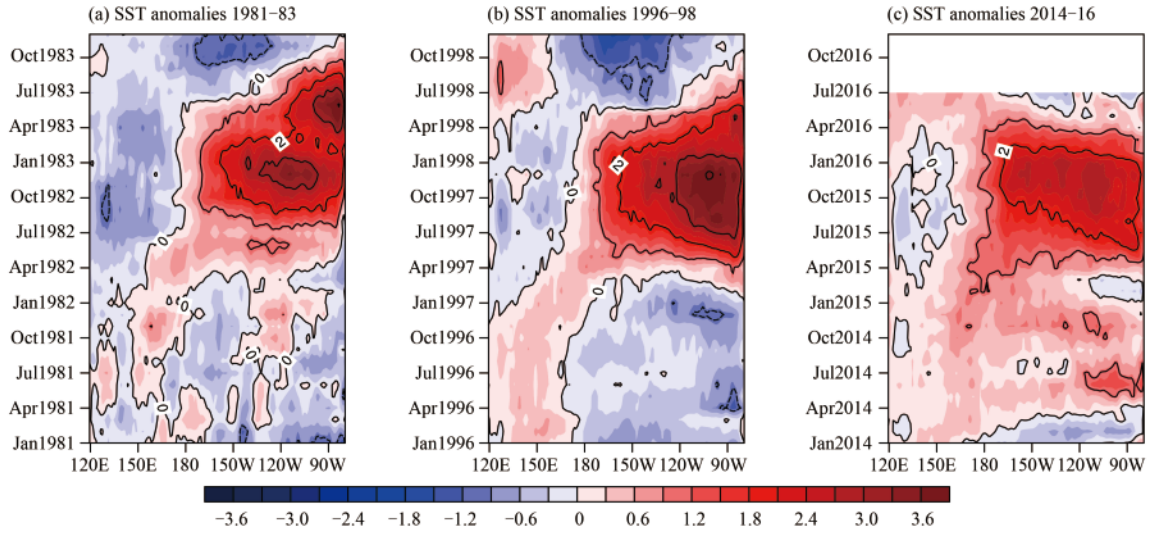

Fig. 1. Time–longitude cross-sections of the Pacific SST anomalies (°C; contour interval: 1°C) averaged over 5°S–5°N for the three super El Niño events.

Table 1. Peak times and values in terms of the Niño3.4 index (°C) for the three super El Niño events, based on the three SST datasets

	ERSST		OISST		HadISST	
Event	Peak time	Peak value	Peak time	Peak value	Peak time	Peak value
1982/83	December 1982	2.14	January 1983	2.79	January 1983	2.46
1997/98	November 1997	2.33	December 1997	2.69	November 1997	2.45
2015/16	November 2015	2.37	November 2015	2.95	November 2015	2.59

Table 2. As in Table 1, but for the Niño3 index

	ERSST		OISST		HadISST	
Event	Peak time	Peak value	Peak time	Peak value	Peak time	Peak value
1982/83	December 1982	2.68	January 1983	3.29	December 1982	3.09
1997/98	November 1997	3.10	December 1997	3.62	December 1997	3.26
2015/16	November 2015	2.53	November 2015	2.93	December 2015	2.65

However, in the decay stage, the features of the three events are not consistent. In the 82/83 and 97/98 events, the positive SST anomaly centers were maintained in eastern Pacific, where the anomalies near the eastern boundary could last until the following summer; whereas during the decay stage of the 15/16 event, the positive center shifted slightly westwards and the positive anomalies east of the dateline delayed at basically the same rate and disappeared earlier at the eastern boundary, compared with the 82/83 and 97/98 events. In the late spring–early summer of 2016, the positive SST anomalies nearly disappeared in the central and eastern equatorial Pacific.

In terms of the horizontal distribution, the 15/16 event had a wider meridional width of positive SST anomalies than the previous two events, and smaller and weaker negative anomalies, as shown in Fig. 2. It is clear that the SST anomalies at the eastern boundary were weaker than in the previous two events, especially in the area south of the equator, and nearly symmetrical with respect to the equator. The features at the equator in Fig. 2 are consistent with Fig. 1.

Figure 3 compares the vertical distributions of equatorial ocean temperature anomalies during the mature

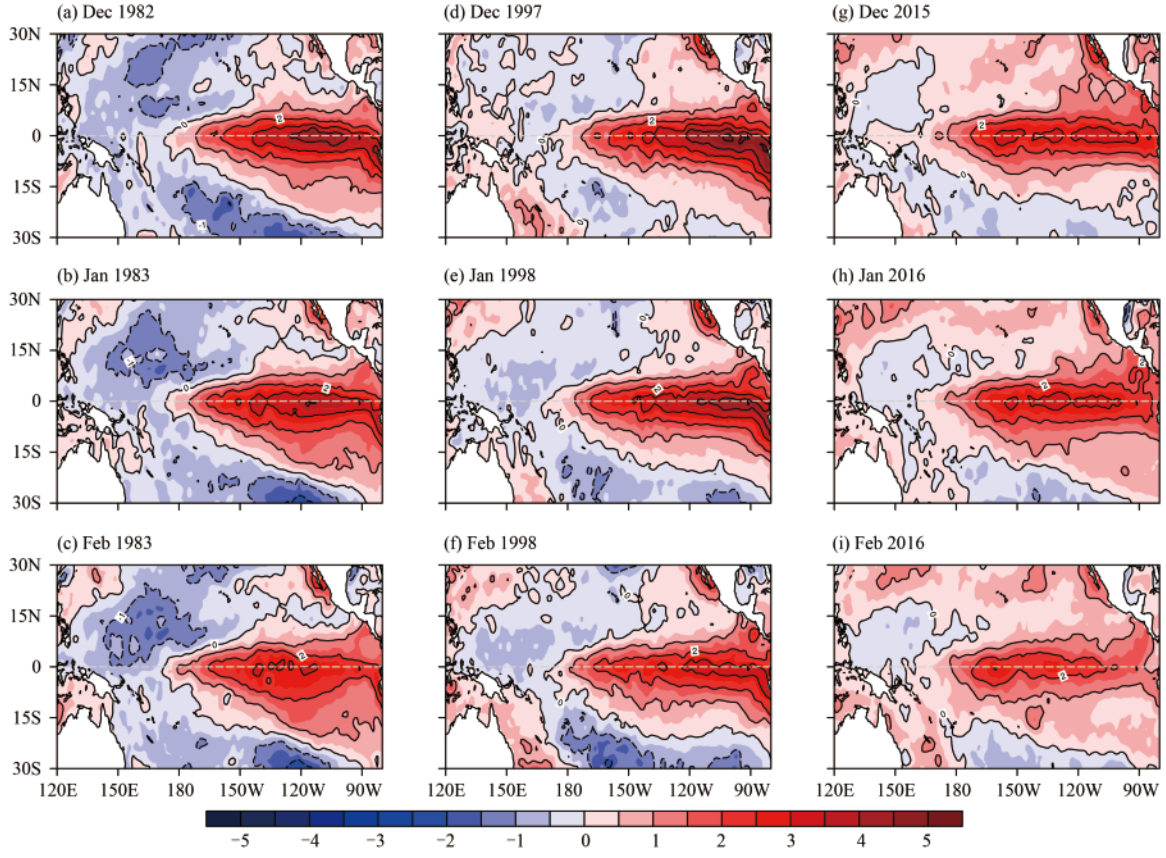

Fig. 2. The SST anomalies (°C; contour interval: 1°C) in December, January, and February during the three super El Niño events.

phase of the three super events. The 15/16 event was different to the two other events insofar as it involved significantly weaker subsurface temperature anomalies. Among the three events, the positive anomalies in the 15/16 event delayed fastest, but had the greatest westward extension over western Pacific. The positive subsurface anomalies in eastern Pacific peaked around November 2015 and began to turn negative in January 2016; whereas, at the same time, both the 82/83 and 97/98 events still maintained strong positive anomalies. Since the center of the positive ocean temperature anomalies did not reach the eastern boundary, the intensity of the SST anomalies near the eastern boundary was much weaker than in the previous two events.

4. Comparison of dynamical features in the upper ocean

4.1 *Thermocline and surface wind stress*

In the air–sea coupled system over western tropical Pacific, changes in upper-ocean dynamical processes are closely related to surface wind events, which plays an important role in ENSO diversity changes (e.g., Chen et al., 2015). The phenomenon of western Pacific westerly wind bursts, due to various external factors, tends to ex-

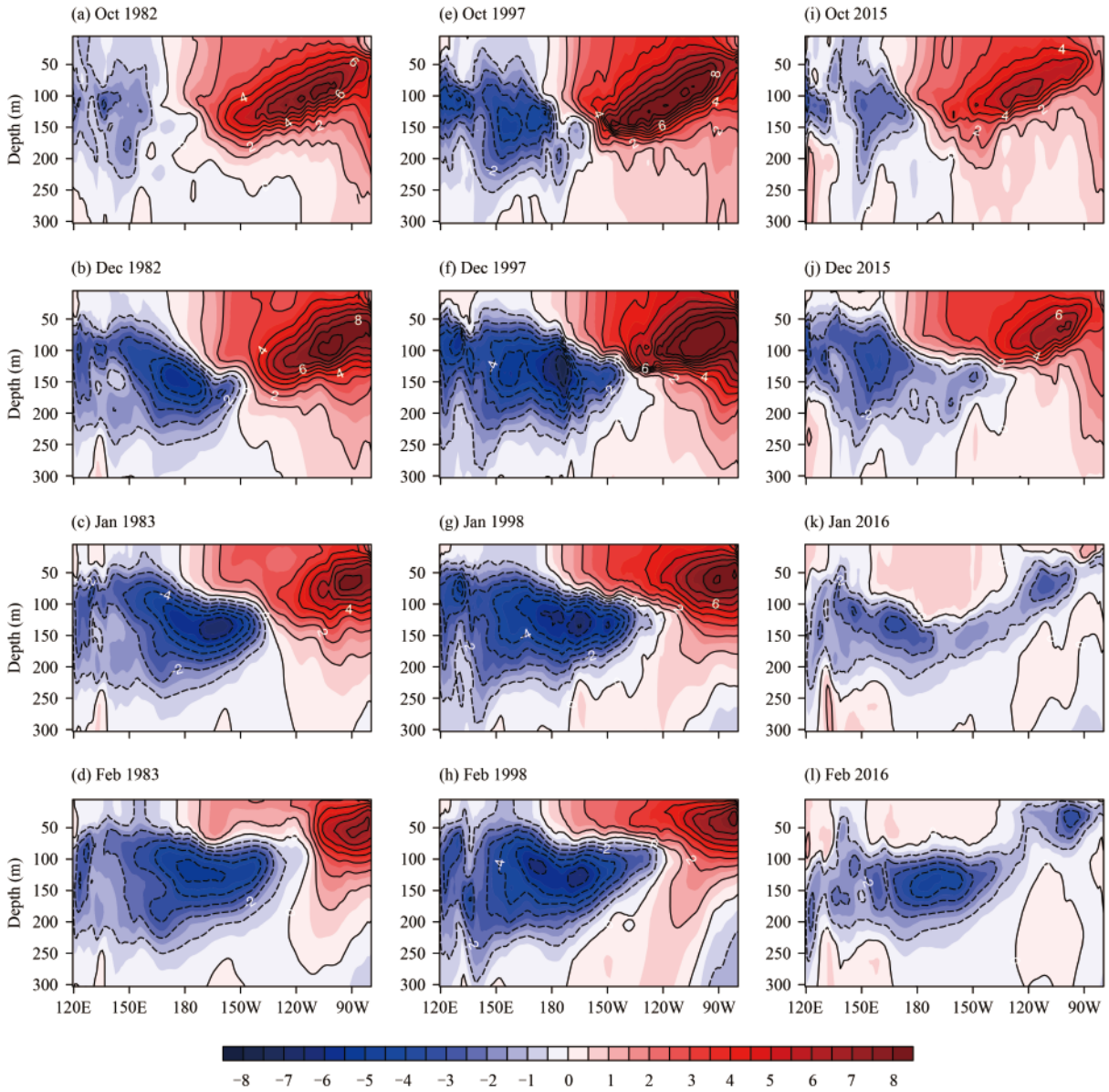

Fig. 3. Longitude–depth cross-sections of ocean temperature anomalies (°C; contour interval: 1°C) averaged over 2°S–2°N in selected months during the three super El Niño events.

cite eastward-propagating equatorial oceanic Kelvin waves, in turn leading to changes in ocean subsurface temperature, and then triggering the thermocline feedback mechanism to form El Niño. Here, we analyze the features of the thermocline and surface wind stress anomalies associated with ENSO.

Figure 4 shows the evolutions of the 20°C isotherm depth (D20) anomalies and zonal surface wind stress anomalies, where the D20 anomalies are used to depict thermocline changes. In their development stage, all three events had an adequate recharging process of equatorial upper-ocean heat content, which may be the physical basis for the formation of super El Niño events. In the mature stage, the zonal reversal structure of the 97/98 event is the most remarkable among the three super events, indicating that the 97/98 event had the strongest discharging process. The eastward propagation of positive subsurface temperature anomalies in the warm pool, driven by the westerly wind anomalies in the equatorial western Pacific, is important to the occurrence of El Niño (Chao et al., 2002; Li et al., 2008). During the early development of the three super events, the westerly wind anomalies appeared in the equatorial western Pacific and drove the warm subsurface signals propagating eastwards (Figs. 4b, d, f).

During the development of the 15/16 event, several warm oceanic Kelvin waves propagated eastwards from western Pacific, accompanied by wind stress anomaly events in western–central Pacific (Chen S. F. et al., 2016; Zhai et al., 2016). In the previous two events, the warm signals propagated eastwards and eventually reached the eastern boundary, while this was not the case in the 15/16 event. In 2015, several eastward-propagating warm signals stagnated in eastern Pacific and the positive D20 anomalies near the eastern boundary were evidently weak, where the anomaly center maintained at around 110°W.

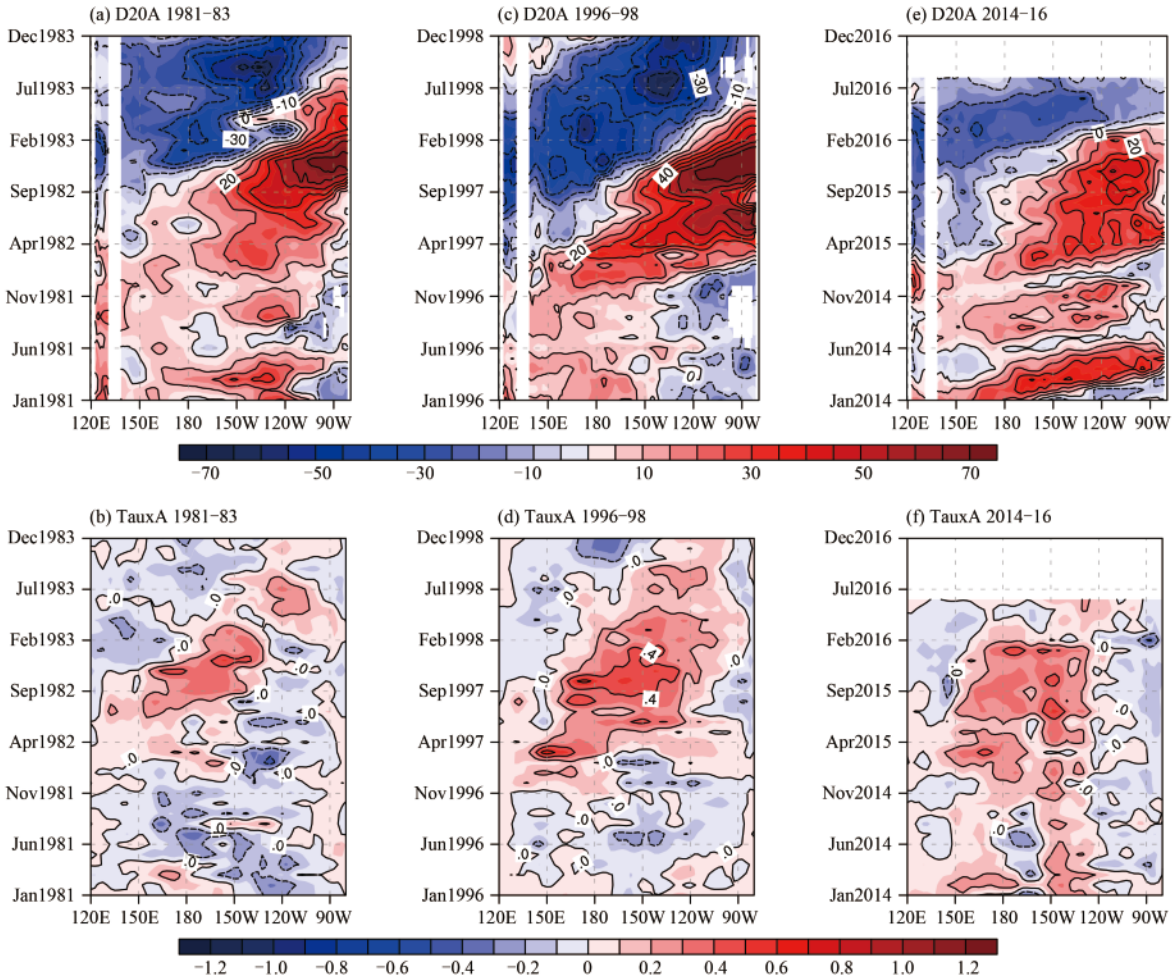

Fig. 4. Time–longitude cross-sections of (a, c, e) the 20°C isotherm depth anomalies (D20A; m; contour interval: 10 m) averaged over 2°S–2°N and (b, d, f) the zonal surface wind stress anomalies (TauxA; 0.1 N m^{-2}; contour interval: 0.02 N m^{-2}) averaged over 5°S–5°N, for the three super El Niño events.

After maturity of this event, the positive D20 anomalies, consistent with the patterns of subsurface temperature anomalies, were much weaker in eastern Pacific compared with the 82/83 and 97/98 events (Fig. 4e). The thermocline changes in El Niño events are connected with surface wind stress anomalies.

In the three events, the changes of the D20 anomalies in the equatorial Pacific before maturity were characterized by two apparent warm oceanic Kelvin waves propagating eastwards and arriving near the eastern boundary around May and December, respectively, where the propagation and stagnation of the Kelvin waves in eastern Pacific were affected by the zonal wind field in this region, especially east of 120°W. In May and December 1997, the equatorial eastern Pacific was dominated by westerly wind anomalies, and the warm signal reached the eastern boundary in the two propagating processes. In 1982, the easterly wind anomalies in eastern Pacific changed from strong to weak, and the warm signal eventually reached the eastern boundary. Since April 2015, easterly wind anomalies had dominated east of 120°W. The warm ocean signals were blocked and did not reach the eastern boundary in the whole of 2015. The strong easterly wind anomalies in eastern Pacific may have been the reason that warm oceanic Kelvin waves stopped propagating eastwards. In the second half of 2015, the easterly wind anomalies promoted cold water upwelling near the eastern boundary, which was unfavorable for the development of positive ocean temperature anomalies and yielded a westward-shifted SST anomaly center in the mature phase. This was the biggest difference between the 15/16 event and the previous two events. But why were the distribution and propagation of surface wind anomalies so different? This remains unclear.

In the development stage, all three events featured rapid eastward propagations of warm oceanic Kelvin waves in the equatorial Pacific, though the Kelvin wave of the 15/16 event featured relatively weak propagation during its mature stage and the off-equatorial oceanic Rossby waves were not so clear as in the previous two events (Fig. 5). These features indicate more or less that the delay oscillator mechanism played roles in these events (Suarez and Schopf, 1988; Battisti and Hirst, 1989). Moreover, the discharging processes of upper-ocean heat content of the three events in the development and ma-

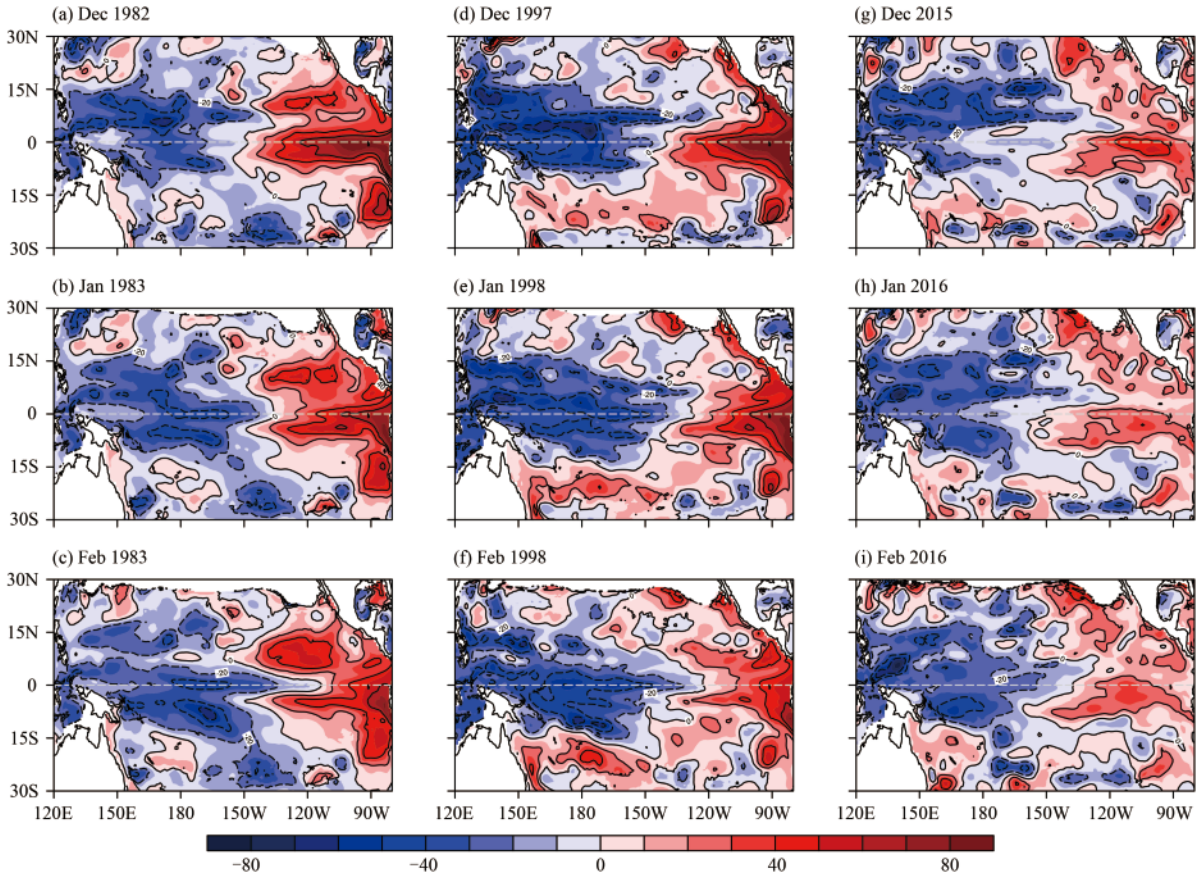

Fig. 5. As in Fig. 2, but for the D20A (contour interval: 20 m).

ture phases were evident (Figs. 4, 5); and in the decaying spring–summer, equatorial zonally uniform patterns of negative heat content anomalies formed, reflecting that the recharge oscillator mechanism was at work in the growth and phase transition of these events (Jin, 1997; Jin and An, 1999).

4.2 *Ocean surface currents and vertical upwelling*

ENSO development is closely connected with variations in anomalous upper-ocean currents, which can affect SST anomalies via zonal advective feedback and Ekman feedback. Owing to the limited length of the OSCAR dataset, we only show the evolution of the ocean surface current anomalies for the 97/98 and 15/16 events (Fig. 6). The zonal current anomalies in the 97/98 event were negative from west to east in the equatorial Pacific (Fig. 6a). These features can also be seen in Fig. 7 and were related to the discharging process of the equatorial heat content anomalies (Ren and Jin, 2013). In contrast, the zonal surface current anomalies in 2015 were weaker and the anomaly center was more westward than that in 1997, which might have led to weaker zonal advective feedback. The positive zonal current anomalies strengthened in early 2015 at the equator, accompanied by en-

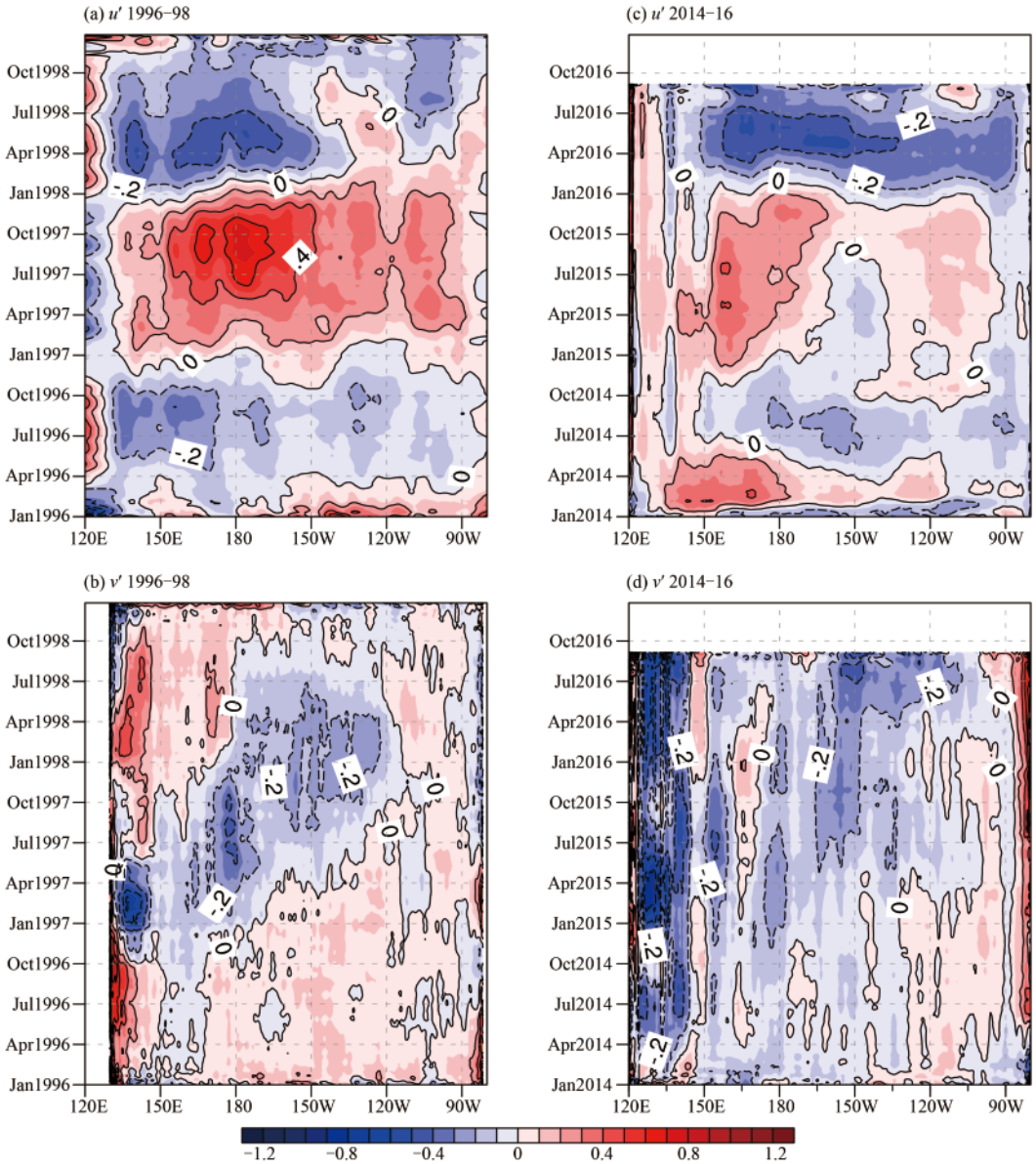

Fig. 6. Time–longitude cross-sections of the OSCAR zonal (u'; m s^{-1}) and meridional (v'; 0.2 m s^{-1}) surface current anomalies (contour interval: 0.2 m s^{-2}; data are smoothed with a 5-month running mean and a zonal 31-point running mean) for the 1997/98 and 2015/16 El Niño events, where u' is averaged over 2°S–2°N and v' is defined in the same domain but by taking the difference between north and south of the equator.

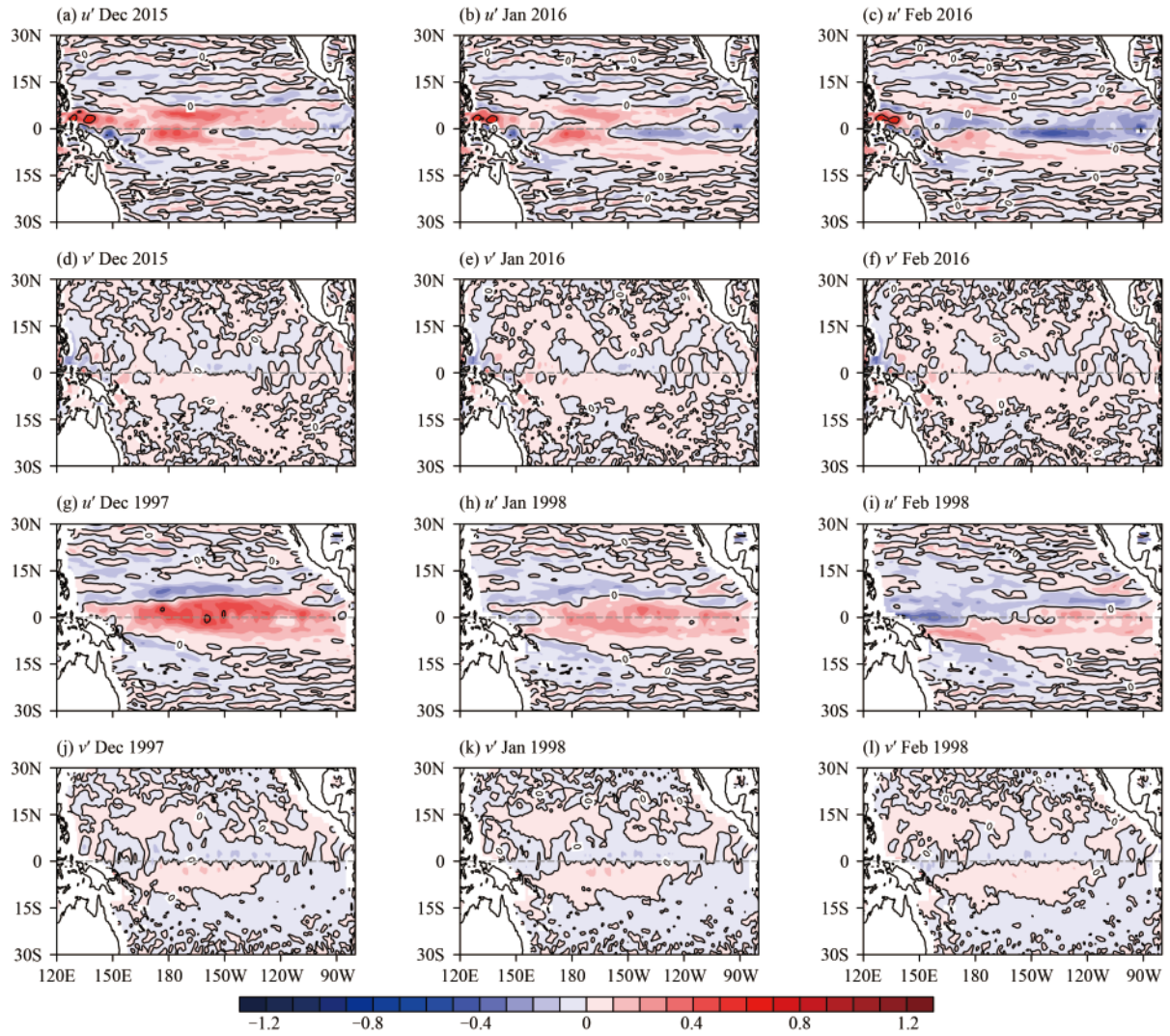

Fig. 7. The OSCAR zonal (u') and meridional (v') surface current anomalies (m s^{-1}; contour interval: 0.5 m s^{-1}; data are smoothed with a 5-month running mean and a 15 × 15-point horizontal running mean) for the 1997/98 and 2015/16 El Niño events.

hanced zonal wind stress anomalies in western Pacific. However, zonal current anomalies were weakly positive over eastern Pacific. In the second half of 2015, the zonal current anomalies turned negative and stretched gradually westwards in the region between 100°W and the eastern boundary (Fig. 6c). The features of the zonal current anomalies in the 15/16 event are unique and cannot be fully explained by the classic recharge oscillator mechanism. One possibility is that it was caused by the invasion of cold water around the eastern boundary, which was accompanied by easterly wind anomalies over eastern Pacific, but it may also be related to the reflection of positive zonal current anomalies at the eastern boundary (Chen H. C. et al., 2016).

The meridional current anomalies both north and south of the equator mainly converged at the equator during these events, and possessed a stronger intensity and wider zonal range in the 15/16 event than in the 97/98 event (Fig. 6d). In the mature stage of the 97/98 event, the meridional current anomalies mainly moved towards the equator west of 120°W, and backwards to the equator in the far eastern Pacific, as seen in Fig. 7. The current anomalies were closely connected with the spatial pattern of anomalous surface wind stress as a response to SST anomalies in the tropical Pacific. In the 15/16 event, the meridional current anomalies mostly converged at the equator, but in the far eastern Pacific and part of western Pacific, they crossed the equator from the south to the north during the mature stage, which may have been related to the northward cross-equatorial flow in this region.

Note that the OSCAR data are relatively short and lack a variable on vertical ocean current. Figure 8 presents the evolution of three-dimensional ocean current anomalies

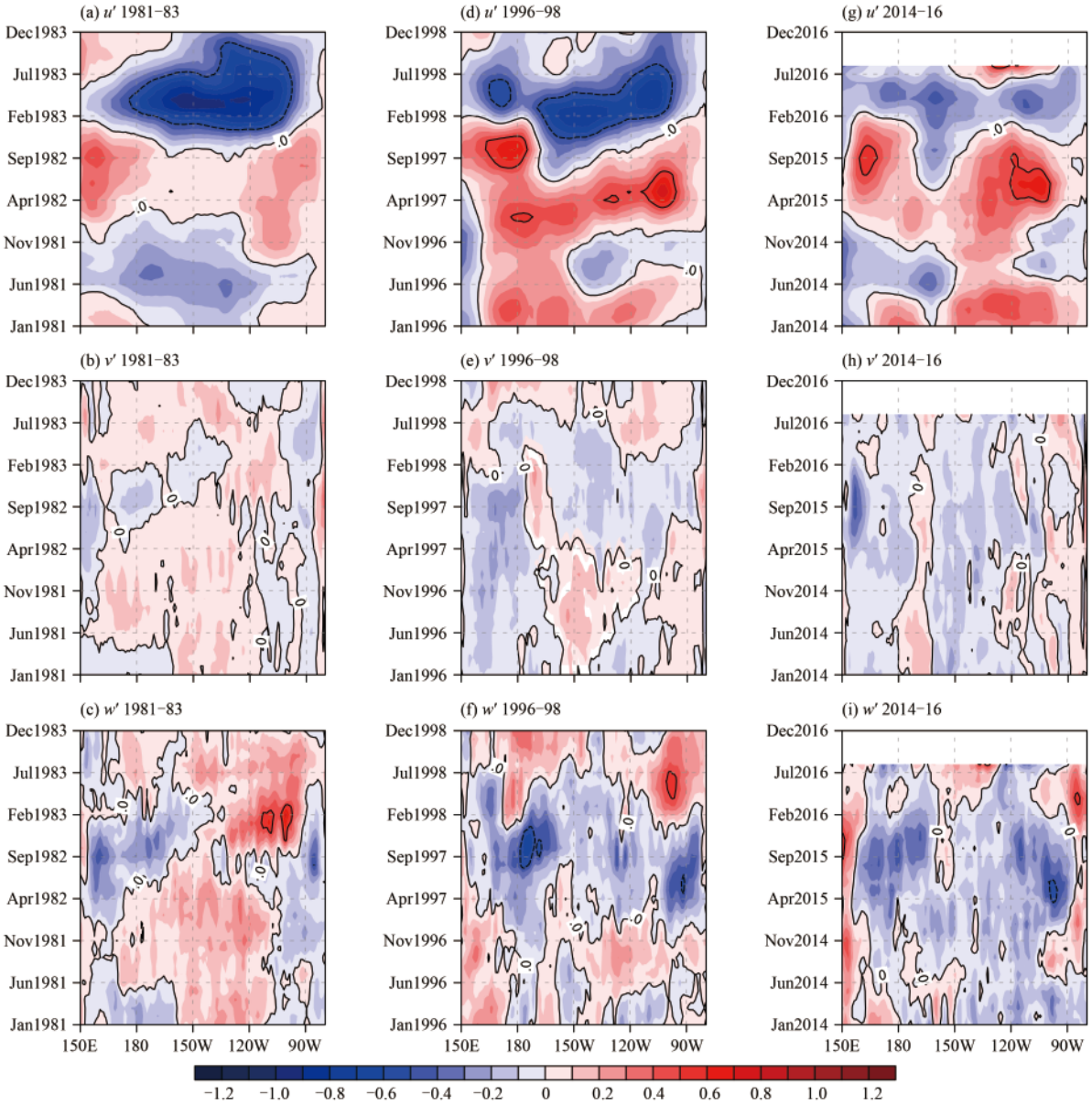

Fig. 8. Time–longitude cross-sections of the GODAS zonal (u'; m s^{-1}), meridional (v'; 0.2 m s^{-1}), and vertical (w'; 2×10^{-5} m s^{-1}) current anomalies (contour interval: 0.5 m s^{-1}; data are smoothed with a 5-month running mean) for the three super El Niño events.

based on the GODAS reanalysis dataset, averaged over the upper 50 m. The features of the GODAS currents are differential from the OSCAR surface currents, especially in the central Pacific, where the negative zonal current anomalies appear in the developing summer. However, the rapidly eastward-propagating meridional current anomalies in Fig. 6 cannot be observed in Fig. 8. Here, in the development stages of the 97/98 and 15/16 events, the currents converged at the equator and downwelling occurred there; however, in the 82/83 event, the currents diverged from the equator and upwelling occurred. From the second half of 2014, the upwelling cold water was slightly enhanced around the eastern boundary (Fig. 8h) and consistent with the features of the OSCAR currents (Fig. 6d), which is the most distinct feature compared with the previous two events at the same stage. In the development and mature stages of the 82/83 and 97/98 events, the cold water upwelling was somewhat suppressed. By contrast, in the 15/16 event, the enhanced upwelling near the eastern boundary and the accompanying easterly wind anomalies in eastern Pacific were probably the direct reason for the zonal current anomalies firstly turning negative in this region.

5. Heat budget analysis in ocean mixed layer

Next, the mixed-layer heat budget for the three events was analyzed, to quantitatively investigate the contribu-

tions of the major oceanic feedbacks to the growth and phase transition of ENSO, as shown in Fig. 9. In general, the features of the 82/83 and 97/98 events are basically similar, which can be used to explain the similarity between their SST anomalies. However, the summation of the five major feedback terms in the 15/16 event had a unique distribution, which was negative over 180°–160°W and near the eastern boundary, and was mainly positive over 160°–90°W. Compared with the previous events, the 15/16 event had a distinct feature in the major terms, with a longer development stage (nearly 2 yr), and its main feedback terms remained negative or positive and featured almost no transitions before the mature stage in most regions, which was not the case in the other two events.

Among the five feedbacks shown in Fig. 9, TH, ZA, and EK are the three positive feedback terms and make positive contributions to the development of super El Niño events, while the MC and TD are negative feedback terms and make negative contributions. On the

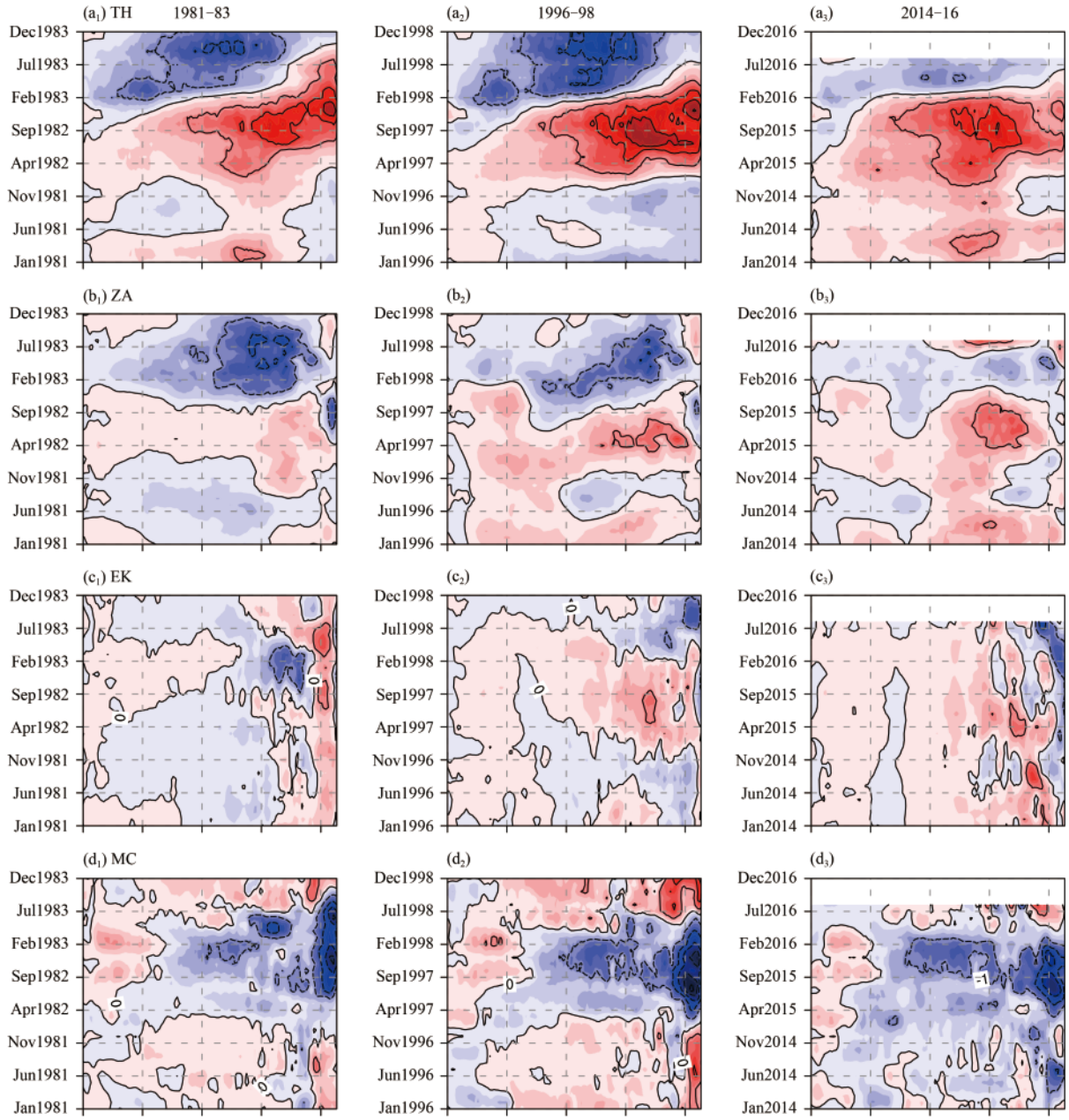

Fig. 9. Time–longitude cross-sections of the mixed-layer dynamical feedback terms (°C month^{-1}; contour interval: 1°C month^{-1}; data are smoothed with a 5-month running mean) for the three super El Niño events, averaged over 2°S–2°N. (a) TH, (b) ZA, (c) EK, (d) MC, (e) TD, and (f) SUM. Left, middle, and right columns represent 1981–83, 1996–98, and 2014–16, respectively.

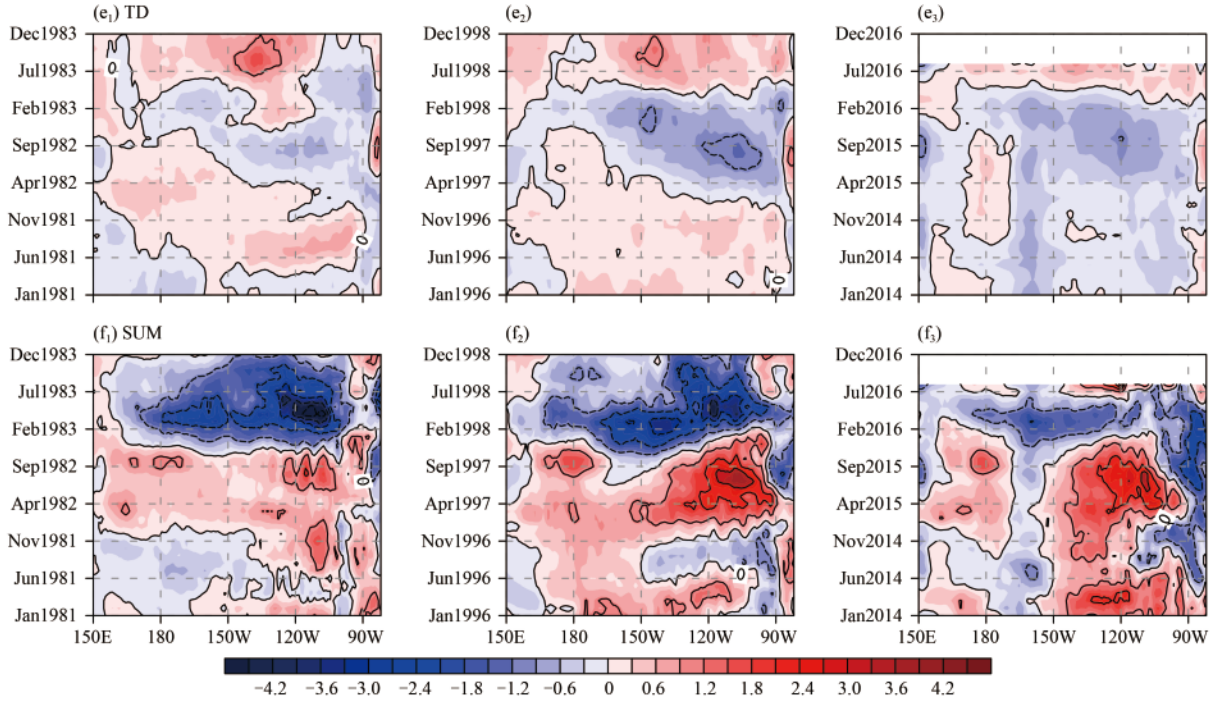

Fig. 9. (Continued.)

whole, TH was the most important positive feedback in the development of the three super events, by providing the main energy source, and also made contributions to the phase transition from El Niño to La Niña due to its peak a few months leading the SST peak. The TH term in the previous two events featured a significantly eastward propagation in the development and mature stages; however, in the 15/16 event, it barely propagated and had weaker amplitude around the eastern boundary, and its positive center was located in the central Pacific. The differences in the TH term among the three events were directly caused by the distribution of subsurface ocean temperature anomalies (Fig. 10). It is clear that, in the Niño3.4 region, the subsurface temperature anomalies were similar in intensity in the 15/16 and 97/98 events. The ZA term is positive but relatively weak in the development stage, and mainly contributes to the phase transition of super El Niño events. It played an important role in the development stage of the 15/16 event, and was stronger than in the previous two events. The contributions of the EK term were generally positive with respect to the growth and phase transitions of the three super events, but with slightly different zonal center positions. In the 15/16 event, the EK term was positive,

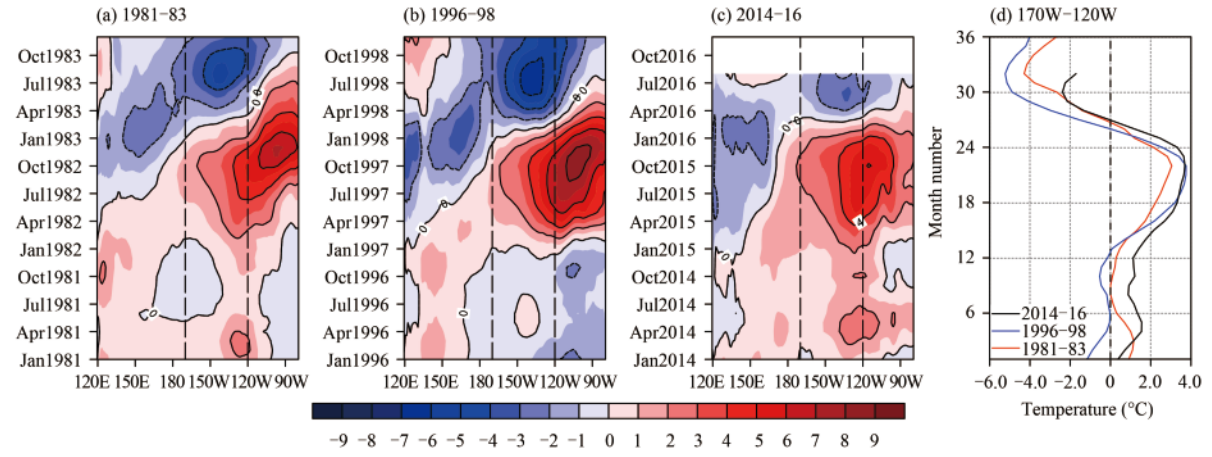

Fig. 10. Time–longitude cross-sections of T'_{sub} (°C; contour interval: 2°C; data are smoothed with a 5-month running mean) for the three El Niño events, where (a–c) are averaged over 2°S–2°N and (d) is averaged over the Niño3.4 region .

mainly east of 120°W, and weak in the western–central Pacific; however, it was negative around the eastern boundary, which have been caused by the cold water upwelling. In addition, the MC and TD terms tend to have fairly similar spatiotemporal patterns and are typically negative feedback terms that are generally out of phase with the SST anomalies, without any contribution to phase transition in the super events. This is because the mean ocean circulation and surface diabatic processes tend to dynamically and thermodynamically damp the mixed layer and SST warming during the development and mature phases of super El Niño events.

Figure 11 further shows the temporal evolutions of the dynamical feedback terms averaged over the Niño3.4 region. Among all the terms of positive feedback, the TH term was the largest, the ZA term was second largest, and then the EK term was weakest. The summations of the five terms were quite similar among the three super events, which reflects their similar phase transitions from warm to cold over the equatorial Pacific. Clearly, the lines of the ZA term are similar to those of the summations. During the development stage of the 15/16 event, the ZA term was positive and stronger than the other two events until the peak stage, which is closely associated with the strength and duration of zonal current anomalies (Fig. 8). It can be seen that, in the 15/16 event, the ZA term not only contributed to phase transition, but also played an important role in the development of this event.

A key question is why the SST anomaly center in the mature stage of the 15/16 event had a significantly westward shift, and the answer may lie in the zonal distributions of the major feedback terms. As shown in Fig. 9, in the mature phase of the 15/16 event, the intensity of the two major positive feedback terms, TH and ZA, did not increased much, but their positive-value centers were westward-shifted and became much weaker in the far eastern Pacific, as compared with the previous two events. Moreover, the negative-value center of the MC term in the 15/16 event was mainly in the far eastern Pacific. All these features would have been favorable for a westward shift of the SST anomaly center in the 15/16 event. In addition, it is also apparent that the TH term turned negative from west to east in the equatorial Pacific during the phase transition stage in the 82/83 and 97/98 events; however, in the 15/16 event, they turned negative, nearly at the same time, over the whole equatorial Pacific.

6. Review of the super El Niño predictions in SEMAP2.0

Based on the aforementioned analyses, both the positive surface wind stress anomalies, corresponding to the westerly wind anomalies, and the thermocline variations, appear to have made crucial contributions to the development and evolution of the super El Niño events, which are also the important preceding signals of ENSO prediction. Therefore, whether or not these two precursors from the thermocline and surface wind stress variations can be effectively used in a prediction approach or system, is key to successfully predicting such super events. To demonstrate this, we briefly introduce the application of these two key precursors in the BCC's prediction system (SEMAP2.0), and examine the performance of the system in predicting the super events.

The development of the 15/16 event was complicated (Shao and Zhou, 2016). In the first half of 2014, the Niño3.4 index quickly increased from –0.5 to 0.5°C. However, in the summer, negative ocean temperature anomalies over southeastern Pacific and the accompanying trade wind anomalies invaded and stagnated the development of positive SST anomalies in the equatorial central–eastern Pacific (Min et al., 2015). After autumn, dynamical processes, including thermocline feedback, promoted warming again in the central Pacific (Fig. 11), and formed a weak central-Pacific El Niño event in the winter. In 2015, El Niño continued to grow quickly and

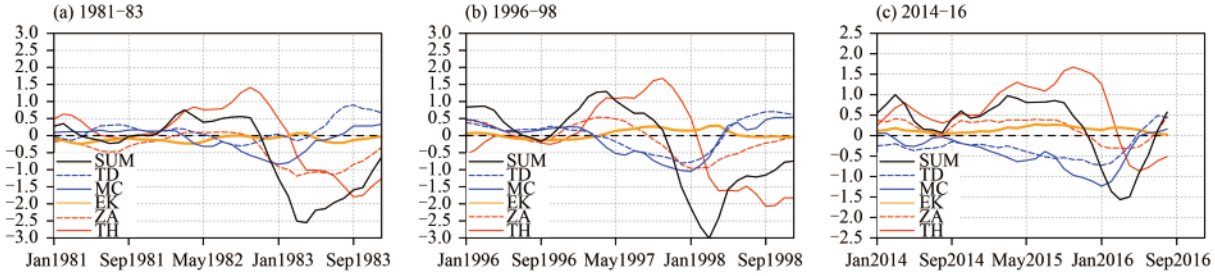

Fig. 11. Temporal evolutions of the dynamical feedback terms (°C month^{-1}; data are smoothed with a five-month running mean) for the three El Niño events averaged over the Niño3.4 region.

transferred from the central-Pacific type into the eastern-Pacific type event. In the early winter of 2015, this super event reached its peak, with a Niño3.4 index value slightly larger than that of the 82/83 and 97/98 events. After the mature phase, this event decayed rapidly and ended in the late spring and early summer of 2016.

Throughout this event, SEMAP2.0 carried out a rolling operational forecast, providing a reference on the prediction of ENSO behavior at the two real-time operational discussion meetings of the BCC during 2014–16. Overall, the forecasts provided by SEMAP2.0 were reasonable and accepted by forecasters (Ren et al., 2016b). Figure 12a presents the results of the three prediction methods in SEMAP2.0, including the BCC_CSM1.1m (CSM) forecast, its analogue-based correction forecast (ADEPS), and the statistical model forecast (STAT) (Ren et al., 2014), along with their multi-method ensemble (MME) mean prediction.

On the one hand, the physics-based statistical prediction model, being mainly based on the recharge oscillator mechanism, can capture the preceding signals in the anomalous evolution of the equatorial Pacific thermocline and western-Pacific westerly anomalies, and also considers the influence of some external precursors of the tropical air–sea system. That is, the persistence of previous SST signals, the variations in the zonally quasi-uniform pattern of thermocline anomalies, the surface wind stress anomalies in the western Pacific, and the Indian Ocean dipole signal, are introduced into the statistical prediction model of Niño indices (Meinen and McPhaden, 2000; Ren et al., 2016b). All the factors of the statistical model are based on the preceding anomalous signals in the oceanic dynamic processes, e.g., the thermocline and surface wind stress anomalies. This statistical model can provide forecasts of the Niño indices, including the Niño3.4 index and the Niño indices of two types of ENSO (Ren and Jin, 2011).

On the other hand, BCC_CSM1.1m can integrate the anomalies of the westerly wind, SST, and subsurface sea temperature, which directly reflect the anomalous signals of the thermocline feedback, into the model prediction by initializing atmospheric forecast variables and three-dimensional ocean temperature. Clearly, both the statistical and dynamical prediction methods have the ability to capture the crucial preceding signals of this super El Niño event. Here, we pay more attention to the performance of the statistical prediction model based on the upper-ocean physical factors and the feedback processes in this super El Niño event, compared with the results of other methods.

From Fig. 12a, it is clear that the curve clusters of predictions by SEMPA2.0 are basically able to cover the actual evolution of the ENSO signal during 2014–16, which is quite good for operational prediction. All of the three prediction methods made reasonable forecasts during the mature and decaying stages, albeit with their own distinct advantages. In general, the climate model predictions and their calibrated forecasts appear to be more skillful for the large amplitude period when the event developed (e.g., the rapidly developing stage of SST anomalies after the spring of 2015). As a comparison, the physics-based statistical model is more effective in capturing the relatively small amplitude periods during the suppressed developing summer and the following au-

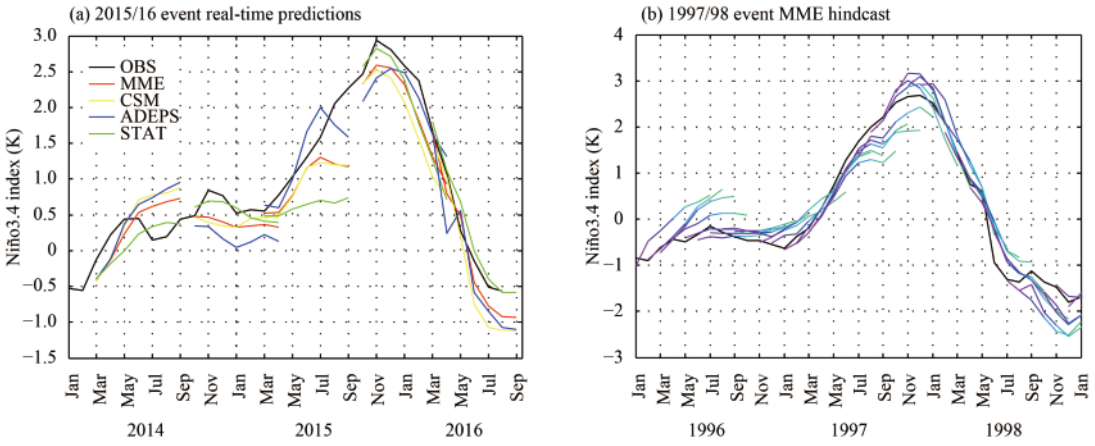

Fig. 12. (a) Plume plot of Niño3.4 index results based on observation (OBS, black curve), as well as the BCC_CSM1.1m (CSM, yellow curve) forecast, its analogue-based correction forecast (ADEPS, blue curve), the statistical model (STAT, green curve), and their multi-method ensemble mean (MME, red curve) prediction in SEMAP2.0, as initiated in each March and October since January 2014. (b) As in (a), but only for the MME-mean predictions, as initiated in each month since January 1996. The predictions initiated in boreal winter, spring, summer, and autumn are indicated by the blue, green, orange, and purple line, respectively.

tumn–winter of 2014, as well as the process of rapid decay and phase transition. As we can see, apart from giving a weak prediction during spring–summer 2015, when the ENSO persistence barrier usually occurs (Ren et al., 2016a), the statistical model better predicted the fluctuations in SST anomaly evolutions of this event by using the preceding variation information of the oceanic precursors. For example, in March 2016, it accurately predicted the weakly cold state at slightly less than –0.5°C, which occurred during August–September 2016 in the central–eastern Pacific. Statistically, the MME mean prediction is generally closer to the observation, and the typical indices of ENSO have also the highest prediction skill scores (Ren et al., 2016b, 2017).

In addition, we used SEMPA2.0 to reforecast the 97/98 event (lack of BCC_CSM1.1 model data before 1991), where the statistical model was trained by utilizing the observed data before 1997. As seen in Fig. 12b, the curve cluster of the MME prediction successfully capture the evolutions of the SST anomalies in the different stages of the event, especially in the transition phase when ENSO is usually difficult to predict; i.e., the forecasts could have been successfully made during the period when SST anomalies were still negative in early 1997. But, we also see that the forecast during the peak time of the 97/98 event is significantly stronger than observed. Overall, throughout the forecasting of the two super ENSO events, SEMAP2.0 showed good performance in predicting these strong events, particularly the processes of rapid decay and phase transition.

7. Summary and discussion

The 15/16 El Niño event has been widely recognized as a super event, comparable to the 82/83 and 97/98 El Niño events, and may well be the strongest event in history in terms of the definition using the Niño3.4 index. Owing to its strong influences on global weather and climate, this new event has been a focus of scientists worldwide. The present study analyzed the evolution of upper-ocean variables in the 15/16 event, compared with the 82/83 and 97/98 super events, and then quantitatively examined the main features of oceanic dynamics in the three super events, as well as the ability to predict them. The conclusions are as follows:

(1) The SST anomalies of the 15/16 event were characterized by an eastward propagation before the mature stage, which was consistent with the previous two super events, but afterwards, turned to a slightly westward propagation. In the development stage of this event, a weak central-Pacific El Niño type event occurred, which then converted to an eastern-Pacific type event in mid-2015. Moreover, the strong easterly wind anomalies in the far eastern Pacific were also a significant feature during the mature phase of this event.

(2) The zonal current anomalies during the transition phase in the 82/83 and 97/98 events turned to negative values from positive, first occurring in the equatorial central–western Pacific. However, in the 15/16 event, such a turning first began over eastern Pacific. This unique feature might have been caused by the easterly wind anomalies in eastern Pacific, which were accompanied by cold water invasion around the eastern boundary.

(3) The upper-ocean positive temperature anomalies in the equatorial Pacific in the 15/16 event were not the strongest among the three super events, but their center was westward-shifted compared with the previous two events. This was closely related to the westward shift of the zonal currents anomalies, which could have led to a stronger zonal advective feedback and favored a westward spatial distribution of ocean temperature anomalies. Both the westward-shifted center of positive subsurface ocean temperature anomalies, compared with the other two events, and the maximum SST anomalies emerging in the Niño3.4 region, indicated that the thermocline feedback may have played the most important role in shaping the unique spatial pattern of the 15/16 event, besides its remarkable contributions to the growth and phase transition of this event.

(4) In the 15/16 event, the oceanic wave activity was remarkably active, accompanied by several westerly wind burst events and eastward-propagating oceanic Kelvin waves. However, unlike the 82/83 and 97/98 events, the equatorial Kelvin waves eventually maintained in eastern Pacific and did not reach the eastern boundary, and the off-equatorial oceanic Rossby waves were not so prominent as those in the previous two events. Indeed, the discharging process of equatorial oceanic heat content was clear in the development and mature stages of this event, and in the decaying spring and following summer, a zonally quasi-uniform pattern of negative heat content anomalies was formed in the equatorial Pacific, reflecting the recharge oscillator mechanism served in the ENSO phase transition.

(5) SEMAP2.0 basically provided reasonable forecasts in the two real-time operational discussion meetings of the BCC each year during 2014–16. In particular, the complex evolutions in the SST anomalies were better predicted by using the statistical prediction model, which considers the preceding anomalous signals in the oceanic precursors, e.g., the thermocline and surface wind stress

anomalies. From the perspective of forecasting stability, the MME mean prediction was more skillful compared to the observation, worthy of being further developed in operational prediction.

Although we have learned about the unique features of oceanic dynamics and feedback processes associated with the 15/16 event, as well as their differences compared to the other two super events, we are still not able to state what primary factors caused this event, and whether these factors could become a predictability source for super El Niño events. The thermocline feedback mechanism was important to the development of these three super events, and may have been a key factor in their formation, which needs to be further studied. In addition, the previous two super events both occurred near moments in time when interdecadal changes of the ENSO regime took place. Previous studies have shown that the two ENSO modes/types feature some evident changes accompanied with observed ENSO interdecadal changes (Ren et al., 2013; Wang and Ren, 2016; Hu et al., 2017). Questions remain as to whether there is a connection between these interdecadal changes and the super event occurrences, and whether the 15/16 super event could be an indicator of the next interdecadal change of ENSO. Still, there are some large uncertainties in the diagnostic analyses based on ocean reanalysis data, due to the lack of ocean observations and deficiencies of ocean models. More comprehensive analysis and exploration are necessary.

Acknowledgments. The authors are grateful to the three anonymous reviewers for their insightful comments, which helped improve the quality of this paper.

REFERENCES

Battisti, D. S., and A. C. Hirst, 1989: Interannual variability in a tropical atmosphere–ocean model: Influence of the basic state, ocean geometry, and nonlinearity. *J. Atmos. Sci.*, **46**, 1687–1712, doi: 10.1175/1520-0469(1989)046<1687:IVIATA>2.0.CO;2.

Behringer, D. W., and Y. Xue, 2004: Evaluation of the global ocean data assimilation system at NCEP: The Pacific ocean. Preprints, Eighth Symposium on Integrated Observing and Assimilation Systems for Atmosphere, Oceans, and Land Surface. Seattle, WA, Amer. Meteor. Soc. 11–15.

Bonjean, F., and G. S. E. Lagerloef, 2002: Diagnostic model and analysis of the surface currents in the tropical Pacific Ocean. *J. Phys. Oceanogr.*, **32**, 2938–2954, doi: 10.1175/1520-0485(2002)032<2938:DMAAOT>2.0.CO;2.

Cane, M. A., M. Münnich, and S. F. Zebiak, 1990: A study of self-excited oscillations of the tropical ocean–atmosphere system. Part I: Linear analysis. *J. Atmos. Sci.*, **47**, 1562–1577, doi: 10.1175/1520-0469(1990)047<1562:ASOSEO>2.0.CO;2.

Chang, P., T. Yamagata, P. Schopf, et al., 2006: Climate fluctuations of tropical coupled systems：The role of ocean dynamics. *J. Climate*, **19**, 5122–5174, doi: 10.1175/JCLI3903.1.

Chao, J. P., S. Y. Yuan, Q. C. Chao, et al., 2002: A data analysis study on the evolution of the El Niño/La Niña cycle. *Adv. Atmos. Sci.*, **19**, 837–844, doi: 10.1007/s00376-002-0048-2.

Chen, D. K., T. Lian, C. B. Fu, et al., 2015: Strong influence of westerly wind bursts on El Niño diversity. *Nature Geoscience*, **8**, 339–345, doi: 10.1038/ngeo2399.

Chen, H. C., Z. Z. Hu, B. H. Huang, et al., 2016: The role of reversed equatorial zonal transport in terminating an ENSO event. *J. Climate*, **29**, 5859–5877, doi: 10.1175/JCLI-D-16-0047.1.

Chen, S. F., R. G. Wu, W. Chen, et al., 2016: Genesis of westerly wind bursts over the equatorial western Pacific during the onset of the strong 2015–2016 El Niño. *Atmos. Sci. Lett.*, **17**, 384–391, doi: 10.1002/asl.2016.17.issue-7.

Chen, W., 2002: Impacts of El Niño and La Niña on the cycle of the East Asian winter and summer monsoon. *Chinese J. Atmos. Sci.*, **26**, 595–610. (in Chinese)

Gasparin, F., and D. H. Roemmich, 2016: The strong freshwater anomaly during the onset of the 2015/2016 El Niño. *Geophys. Res. Lett.*, **43**, 6452–6460, doi: 10.1002/2016GL069542.

Hu, S. N., and A. V. Fedorov, 2016: Exceptionally strong easterly wind burst stalling El Niño of 2014. *Proceedings of the National Academy of Sciences of the United States of America*, **113**, 2005–2010, doi: 10.1073/pnas.1514182113.

Hu, Z.-Z., A. Kumar, B. H. Huang, et al., 2017: Interdecadal variations of ENSO around 1999/2000. *J. Meteor. Res.*, **31**, 73–81, doi: 10.1007/s13351-017-6074-x.

Huang, R. H., R. H. Zhang, and Q. Y. Zhang, 2000: The 1997/98 ENSO cycle and its impact on summer climate anomalies in East Asia. *Adv. Atmos. Sci.*, **17**, 348–362, doi: 10.1007/s00376-000-0028-3.

Jin, F.-F., 1997: An equatorial ocean recharge paradigm for ENSO. Part I: Conceptual model. *J. Atmos. Sci.*, **54**, 811–829, doi: 10.1175/1520-0469(1997)054<0811:AEORPF>2.0.CO;2.

Jin, F.-F., and S.-I. An, 1999: Thermocline and zonal advective feedbacks within the equatorial ocean recharge oscillator model for ENSO. *Geophys. Res. Lett.*, **26**, 2989–2992, doi: 10.1029/1999GL002297.

Kanamitsu, M., W. Ebisuzaki, J. Woollen, et al., 2002: NCEP-DOE AMIP-Ⅱ reanalysis (R-2). *Bull. Amer. Meteor. Soc.*, **83**, 1631–1643, doi: 10.1175/BAMS-83-11-1631.

Levine, A. F. Z., and M. J. McPhaden, 2016: How the July 2014 easterly wind burst gave the 2015–2016 El Niño a head start. *Geophys. Res. Lett.*, **43**, 6503–6510, doi: 10.1002/2016GL069204.

Li, C. Y., 1990: Interaction between anomalous winter monsoon in East Asia and El Niño events. *Adv. Atmos. Sci.*, **7**, 36–46, doi: 10.1007/BF02919166.

Li, C. Y., M. Mu, G. Q. Zhou, et al., 2008: Mechanism and prediction studies of the ENSO. *Chinese J. Atmos. Sci.*, **32**, 761–781. (in Chinese)

Li, Q. Q., and Q. Y. Min, 2016: A dialogue with Renhe Zhang: The heavy rainfall over southern China in the first half year of 2016 and its relation to the 2015/2016 super El Niño. *Chin. Sci. Bull.*, **61**, 2659–2662. (in Chinese)

Liu, Y. M., B. Q. Liu, R. C. Ren, et al., 2016: Current super El Niño event and its impacts on climate in China in spring and

summer. *Bulletin of Chinese Academy of Sciences*, **31**, 241–250. (in Chinese)

Meinen, C. S., and M. J. McPhaden, 2000: Observations of warm water volume changes in the equatorial Pacific and their relationship to El Niño and La Niña. *J. Climate*, **13**, 3551–3559, doi:10.1175/1520-0442(2000)013<3551:OOWWVC>2.0.CO;2.

Min, Q. Y., J. Z. Su, R. H. Zhang, et al., 2015: What hindered the El Niño pattern in 2014? *Geophys. Res. Lett.*, **42**, 6762–6770, doi: 10.1002/2015GL064899.

National Climate Center, 1998: *China Flooding and Climate Anomalies in 1998*. China Meteorology Press, Beijing, 88–108. (in Chinese)

Neelin, J. D., D. S. Battisti, A. S. Hirst, et al., 1998: ENSO theory. *J. Geophys. Res.*, **103**(C7), 14261–14290, doi: 10.1029/97JC03424.

Picaut, J., F. Masia, and Y. du Penhoat, 1997: An advective-reflective conceptual model for the oscillatory nature of the ENSO. *Science*, **277**, 663–666, doi: 10.1126/science.277.5326.663.

Rayner, N. A., D. E. Parker, E. B. Horton, et al., 2003: Global analyses of sea surface temperature, sea ice, and night marine air temperature since the late nineteenth century. *J. Geophys. Res.*, **108**, 4407, doi: 10.1029/2002JD002670.

Ren, H.-L., and F.-F. Jin, 2011: Niño indices for two types of ENSO. *Geophys. Res. Lett.*, **38**, L04704, doi: 10.1029/2010GL046031.

Ren, H.-L., and F.-F. Jin, 2013: Recharge oscillator mechanisms in two types of ENSO. *J. Climate*, **26**, 6506–6523, doi: 10.1175/JCLI-D-12-00601.1.

Ren, H.-L., F.-F. Jin, M. F. Stuecker, et al., 2013: ENSO regime change since the late 1970s as manifested by two types of ENSO. *J. Meteor. Soc. Japan*, **91**, 835–842, doi: 10.2151/jmsj.2013-608.

Ren, H.-L., Y. Liu, F. F. Jin, et al., 2014: Application of the analogue-based correction of errors method in ENSO prediction. *Atmos. Oceanic Sci. Lett.*, **7**, 157–161, doi: 10.1080/16742834.2014.11447152.

Ren, H.-L., F.-F. Jin, B. Tian, et al., 2016a: Distinct persistence barriers in two types of ENSO. *Geophys. Res. Lett.*, **43**, 10973–10979, doi: 10.1002/2016GL071015.

Ren, H.-L., Y. Liu, J. Q. Zuo, et al., 2016b: The new generation of ENSO prediction system in Beijing Climate Center and its predictions for the 2014/2016 super El Niño event. *Meteor. Mon.*, **42**, 521–531. (in Chinese)

Ren, H.-L., F.-F. Jin, L. C. Song, et al., 2017: Prediction of primary climate variability modes in Beijing Climate Center. *J. Meteor. Res.*, **31**, 204–223, doi: 10.1007/s13351-017-6097-3.

Shao, X., and B. Zhou, 2016: Monitoring and diagnosis of the 2015/2016 super El Niño event. *Meteor. Mon.*, **42**, 540–547. (in Chinese)

Stramma, L., T. Fischer, D. S. Grundle, et al., 2016: Observed El Niño conditions in the eastern tropical Pacific in October 2015. *Ocean Science*, **12**, 861–873, doi: 10.5194/os-12-861-2016.

Stuecker, M. F., A. Timmermann, F.-F. Jin, et al., 2013: A combination mode of the annual cycle and the El Niño/Southern Oscillation. *Nature Geoscience*, **6**, 540–544, doi: 10.1038/ngeo1826.

Suarez, M. J., and P. S. Schopf, 1988: A delayed action oscillator for ENSO. *J. Atmos. Sci.*, **45**, 3283–3287, doi: 10.1175/1520-0469(1988)045<3283:ADAOFE>2.0.CO;2.

Wang, B., R. G. Wu, and X. H. Fu, 2000: Pacific–East Asian teleconnection: How does ENSO affect east Asian climate? *J.Climate*, **13**, 1517–1536, doi: 10.1175/1520-0442(2000)013<1517:PEATHD>2.0.CO;2.

Wang, R., and H.-L. Ren, 2016: The linkage between two ENSO types/modes and the interdecadal changes of ENSO around the year 2000. *Atmos. Oceanic Sci. Lett.*, **10**, 168–174, doi: 10.1080/16742834.2016.1258952.

Weisberg, R. H., and C. Z. Wang, 1997: A western Pacific oscillator paradigm for the El Niño–Southern Oscillation. *Geophys. Res. Lett.*, **24**, 779–782, doi: 10.1029/97GL00689.

Xie, S.-P., Y. Kosaka, Y. Du, et al., 2016: Indo–western Pacific Ocean capacitor and coherent climate anomalies in post-ENSO summer: A review. *Adv. Atmos. Sci.*, **33**, 411–432, doi: 10.1007/s00376-015-5192-6.

Yuan, Y., H. Gao, X. L. Jia, et al., 2016: Influences of the 2014–2016 super El Niño event on climate. *Meteor. Mon.*, **42**, 532–539. (in Chinese)

Zhai, P. M., R. Yu, Y. J. Guo, et al., 2016: The strong El Niño of 2015/16 and its dominant impacts on global and China's climate. *J. Meteor. Res.*, **30**, 283–297, doi: 10.1007/s13351-016-6101-3.

Zhang, Q., A. Kumar, Y. Xue, et al., 2007: Analysis of the ENSO cycle in the NCEP coupled forecast model. *J. Climate*, **20**, 1265–1284, doi: 10.1175/JCLI4062.1.

Zhang, R. H., A. Sumi, and M. Kimoto, 1996: Impact of El Niño on the East Asian monsoon: A diagnostic study of the '86/87 and '91/92 events. *J. Meteor. Soc. Japan*, **74**, 49–62.

Zhang, W. J., F.-F. Jin, J. P. Li, et al., 2011: Contrasting impacts of two-type El Niño over the western North Pacific during boreal autumn. *J. Meteor. Soc. Japan*, **89**, 563–569, doi: 10.2151/jmsj.2011-510.

Zhang, W. J., F.-F. Jin, H.-L. Ren, et al., 2012: Differences in teleconnection over North Pacific and rainfall shift over the USA associated with two types of El Niño during boreal autumn. *J. Meteor. Soc. Japan*, **90**, 535–552, doi: 10.2151/jmsj.2012-407.

Tech & Copy Editor: Zhirong CHEN
Language Editor: Colin SMITH